Electronic Supplementary Information

Plasma-assisted rhodium incorporation in nickel-iron sulfide nanosheets: enhanced catalytic activity and Janus mechanism for overall water splitting

Junying Li [a], Xiaodeng Wang [b,*], Lingya Yi [a], Changxiang Fang [a], Tianhao Li [a], Wei Sun [c,*] and Weihua Hu [a,*]

[a] Key Laboratory of Luminescence Analysis and Molecular Sensing (Southwest University), Ministry of Education; School of Materials and Energy, Chongqing Key Laboratory for Advanced Materials and Technologies of Clean Energies, Southwest University, Chongqing 400715, China

E-mail: whhu@swu.edu.cn (W. Hu)

[b] Chongqing Engineering Research Center of New Energy Storage Devices and Applications, Chongqing University of Arts and Sciences, Chongqing, 402160, China.

E-mail: wangxd@cqwu.edu.cn (X. Wang)

[c] Key Laboratory of Laser Technology and Optoelectronic Functional Materials of Hainan Province, Key Laboratory of Functional Materials and Photoelectrochemistry of Haikou, College of Chemistry and Chemical Engineering, Hainan Normal University, Haikou 571158, China

E-mail: sunwei@hainnu.edu.cn (W. Sun).

1. DFT calculation.

For HER, The free energy for hydrogen adsorption (ΔG_{H*}) was calculated according to the equation as follows:[1]

$$\Delta G_{H*} = \Delta E_H + \Delta E_{ZPE} - T\Delta S_H$$

where * designates a surface adsorbed specie and ΔE_H is H chemisorption energy. ΔS_H and ΔE_{ZPE} are the differences in entropy and zero-point energy between the adsorbed H* and gas phase H_2. The value of ΔE_{ZPE}-$T\Delta S_H$ at a temperature (T) of 300 K. [2]

The water dissociation energy was calculated by the following equation: [3]

$$E_{dissociation} = E_{H2O*} - E_{H*+OH*}$$

where E_{H2O*} and E_{H*+OH*} represent the total surface energies with H_2O that adsorbed on the pristine surface and that of H*and OH*, respectively.

For OER process, we calculate the Gibbs free energy of coordinate elementary steps and overpotential for OER based on the following 4e mechanism proposed by Norskov for water oxidation, which include of the following four elementary steps: [4]

$$OH^- + * \rightarrow *OH + e^-$$

$$*OH + OH^- \rightarrow *O + H_2O + e^-$$

$$*O + OH^- \rightarrow *OOH + e^-$$

$$*OOH + OH^- \rightarrow * + O_2 + H_2O + e^-$$

where * denotes the active sites on the catalyst surface. The computational hydrogen electrode model was used to calculate the free energies of OER. The free energy of the adsorbed species is defined as

$$\Delta G_{ads} = \Delta E_{ads} + \Delta E_{ZPE} - T\Delta S_{ads}$$

where ΔE_{ads} is the electronic adsorption energy, ΔE_{ZPE} is the zero point energy difference between the adsorbed and gaseous species, and $T\Delta S_{ads}$ is the corresponding entropy difference between these two states. The electronic binding energy is referenced as $\frac{1}{2}H_2$ for each H atom, and (H_2O–H_2) for each O atom, plus the energy of the clean slab.

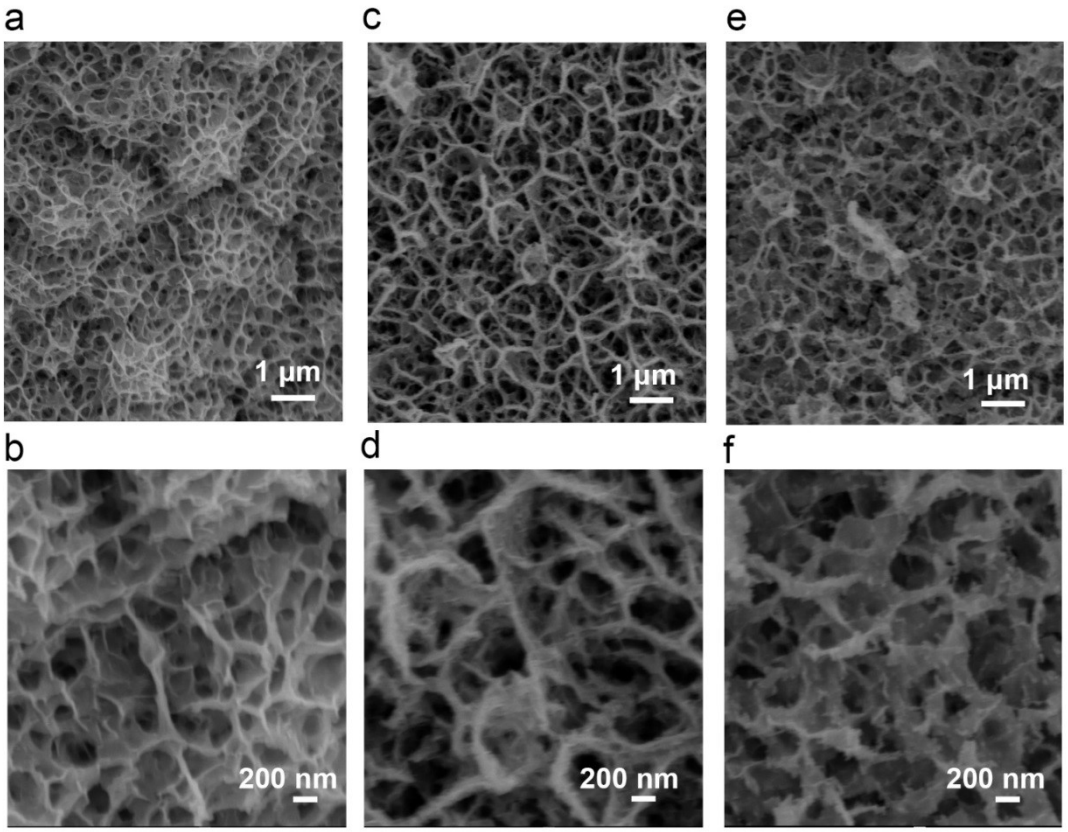

Fig. S1. SEM images of *p*-Rh/Fe-Ni_3S_2/NF synthesized with H_2 plasma treatment of 10 min (a and b), 20 min (c and d), and 30 min (e and f), respectively.

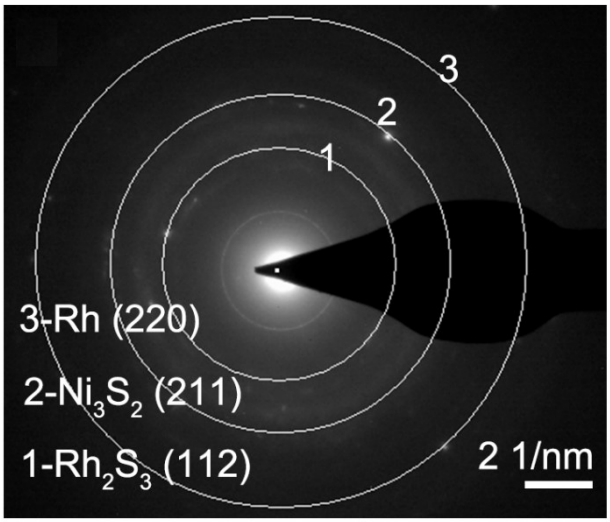

Fig. S2. SAED pattern of *p*-Rh/Fe-Ni_3S_2/NF.

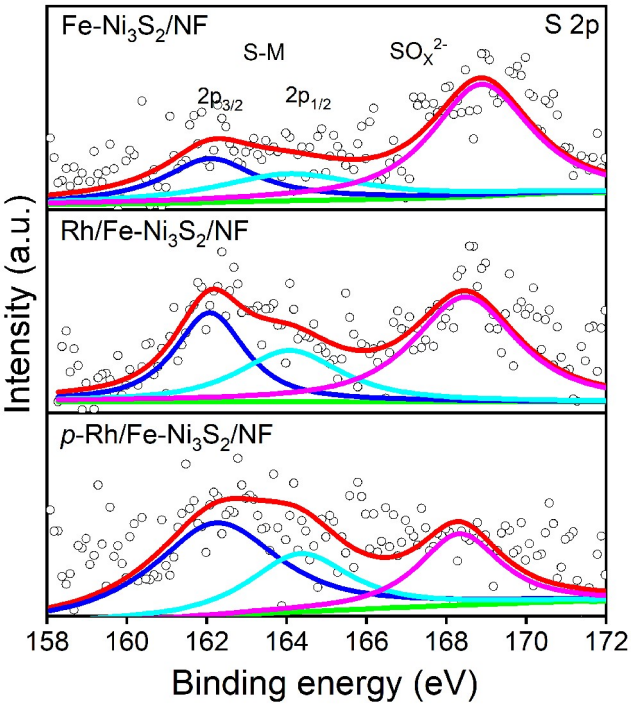

Fig. S3. S 2p XPS spectra of *p*-Rh/Fe-Ni_3S_2/NF in comparison to Fe-Ni_3S_2/NF, Rh/Fe-Ni_3S_2/NF.

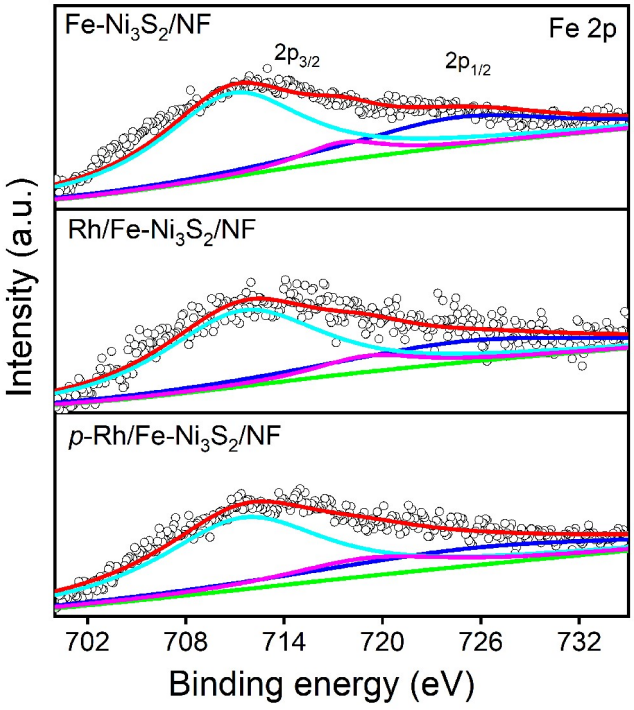

Fig. S4. Fe 2p XPS spectra of *p*-Rh/Fe-Ni_3S_2/NF in comparison to Fe-Ni_3S_2/NF, Rh/Fe-Ni_3S_2/NF.

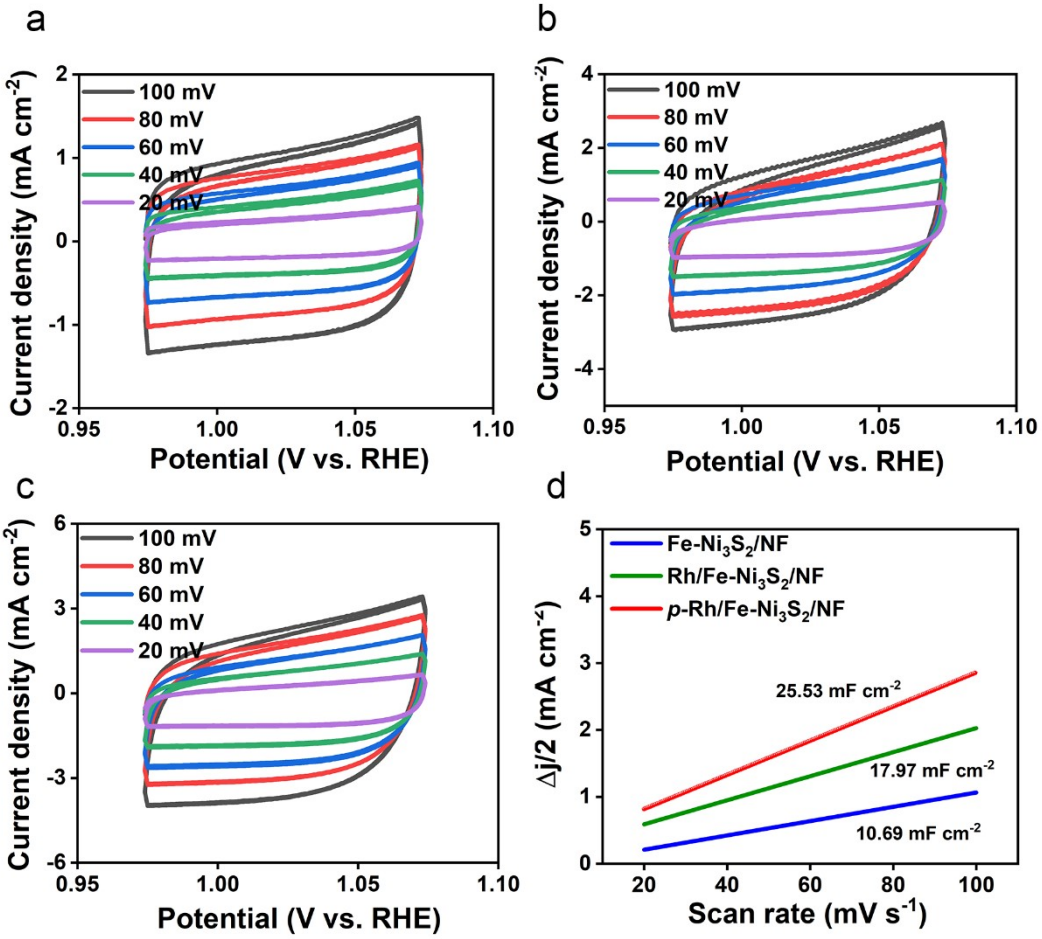

Fig. S5. CV curves of Fe-Ni_3S_2/NF (a), Rh/Fe-Ni_3S_2/NF (b), and *p*-Rh/Fe-Ni_3S_2/NF (c) with scan rates ranging from 20 to 100 mV s^{-1} after OER test. By plotting the capacitive currents (ΔJ, $(J_a-J_c)/2$) against the scanning rate and following with a linear fit, the C_{dl} was estimated as the slope. (d) Plots of capacitive current vs. scanning rate and calcuated electrochemical double-layer capacitanc (C_{dl}).

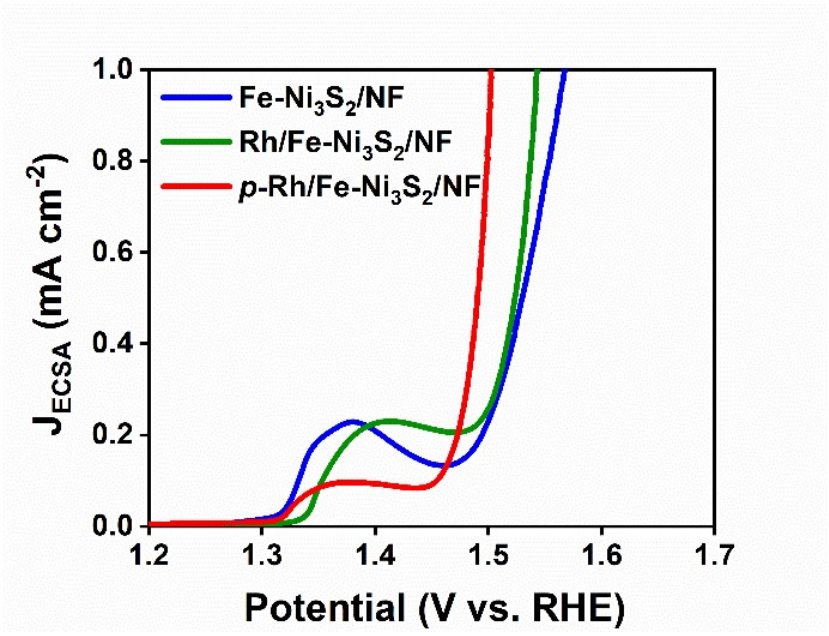

Fig. S6. ECSA-normalized LSV curves of Fe-Ni_3S_2/NF, Rh/Fe-Ni_3S_2/NF, and *p*-Rh/Fe-Ni_3S_2/NF in OER. (The C_{dl} was further converted into ECSA using the specific capacitance value for a flat surface of 0.04 mF cm^{-2}).

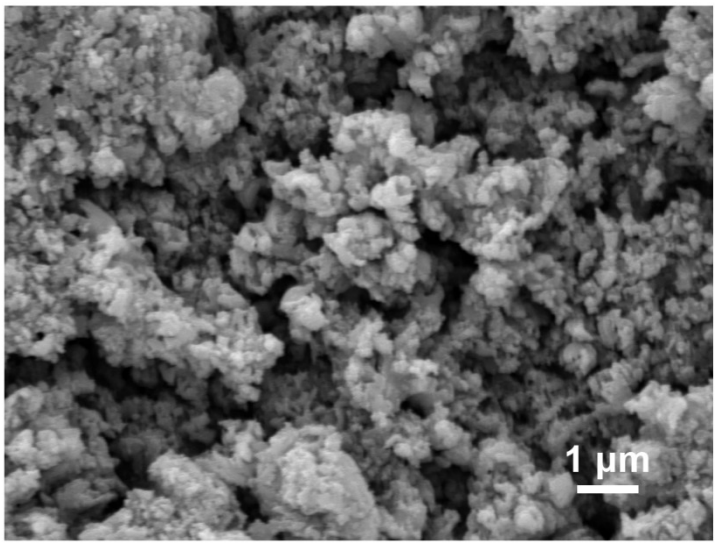

Fig. S7. SEM image of *p*-Rh/Fe-Ni_3S_2/NF after 50 h OER at 100 mA cm^{-2}.

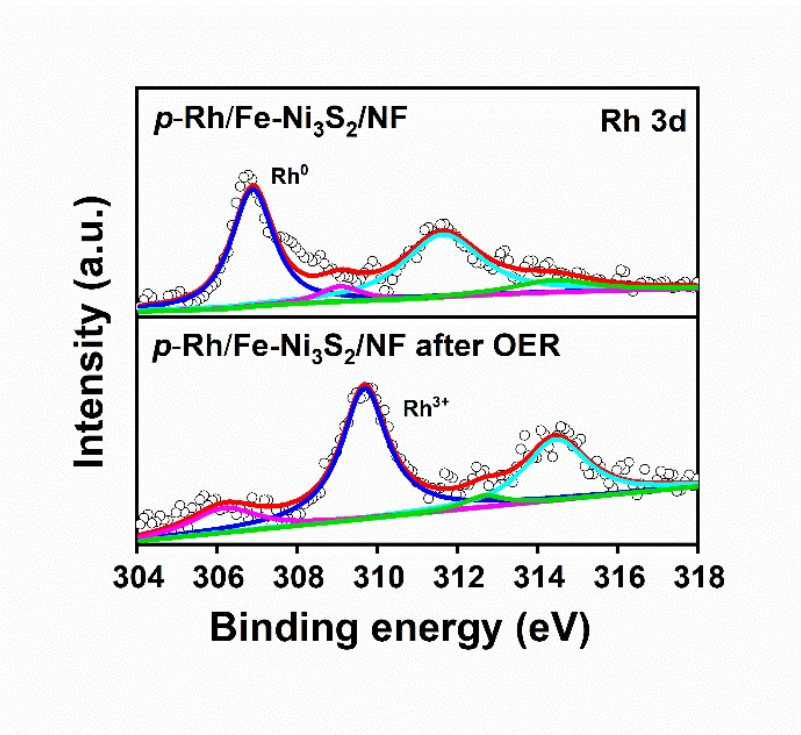

Fig. S8. Rh 3d XPS of *p*-Rh/Fe-Ni_3S_2/NF after 50 h OER at 100 mA cm^{-2}.

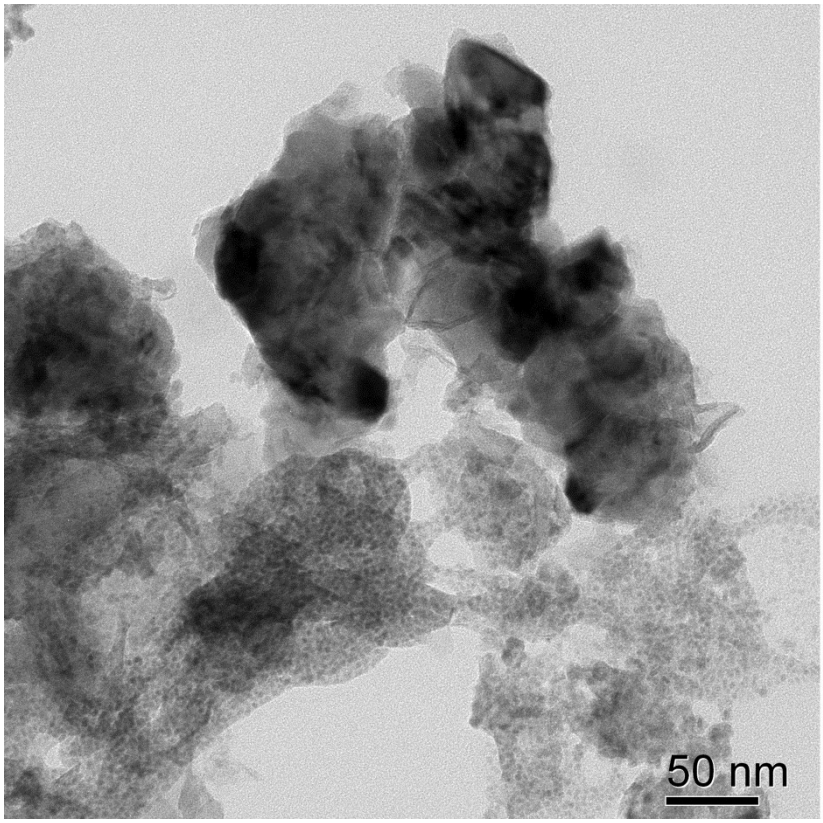

Fig. S9. TEM image of *p*-Rh/Fe-Ni_3S_2/NF after 50 h OER at 100 mA cm^{-2}.

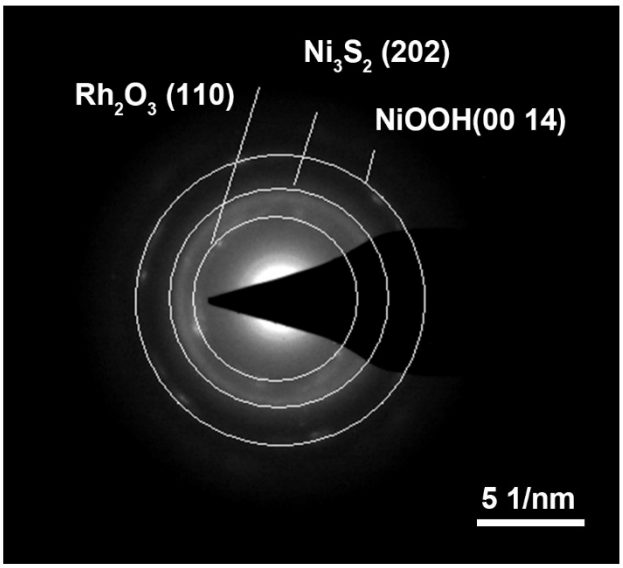

Fig. S10. SAED pattern of *p*-Rh/Fe-Ni_3S_2/NF after 50 h OER at 100 mA cm^{-2}.

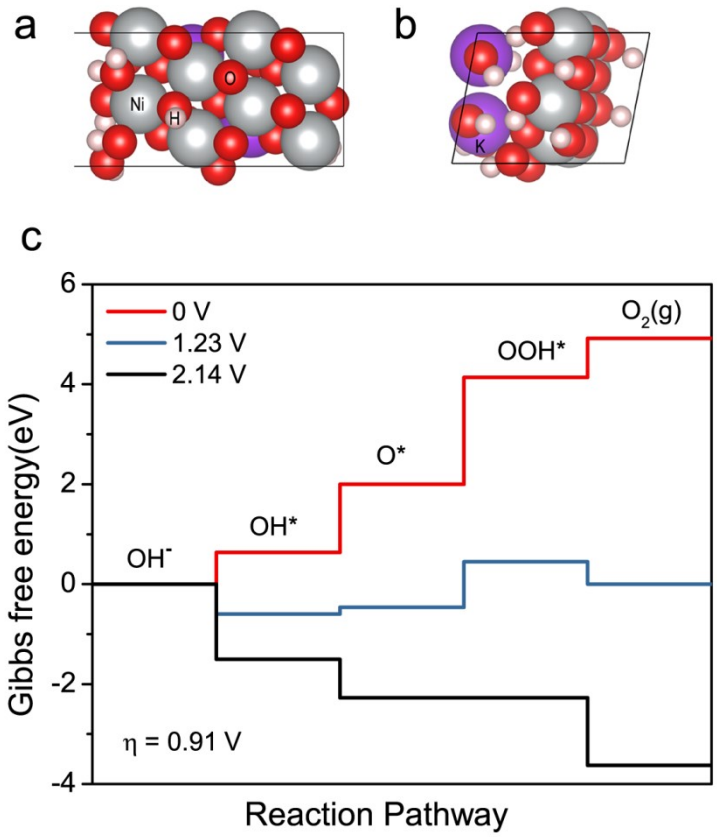

Fig. S11. DFT calculation of OER process on NiOOH. Side (a) and top view (b) of the model surface; Free energy diagrams of OER (c).

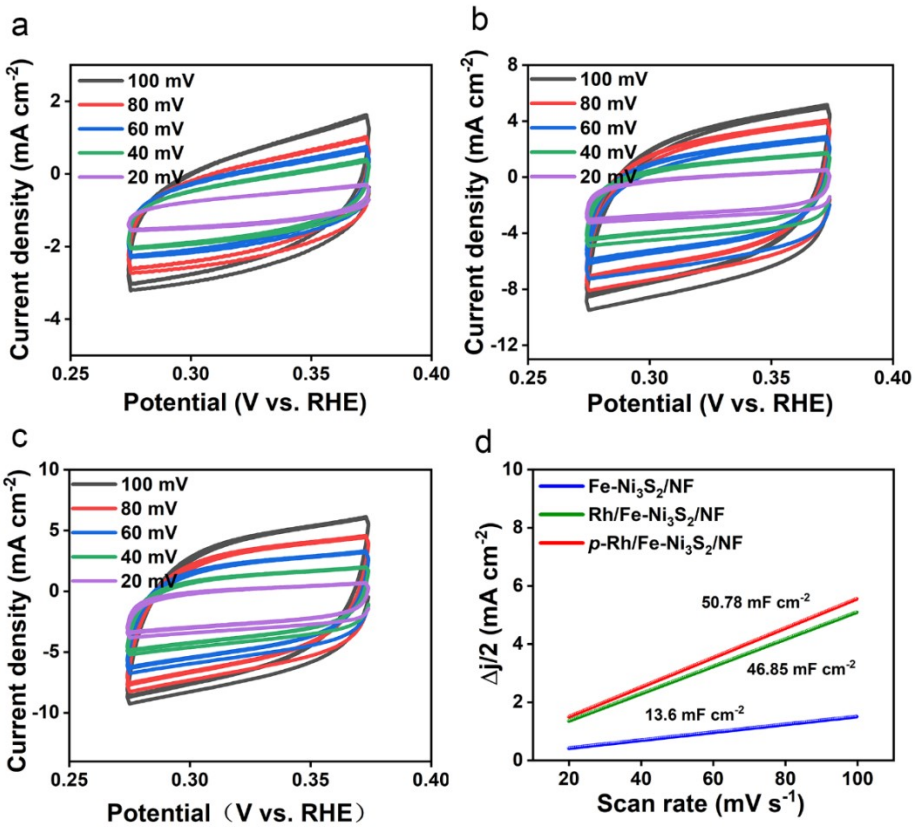

Fig. S12. CV curves of Fe-Ni_3S_2/NF (a), Rh/Fe-Ni_3S_2/NF (b), and *p*-Rh/Fe-Ni_3S_2/NF (c) with scan rates ranging from 20 to 100 mV s^{-1} after HER test. (d) Plots of capacitive current vs. Scanning rate and calcuated electrochemical double-layer capacitanc (C_{dl}).

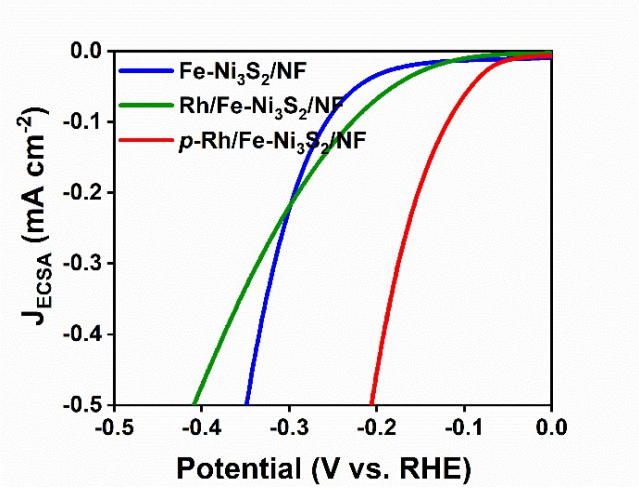

Fig. S13. ECSA-normalized LSV curves of Fe-Ni_3S_2/NF, Rh/Fe-Ni_3S_2/NF, and *p*-Rh/Fe-Ni_3S_2/NF for HER.

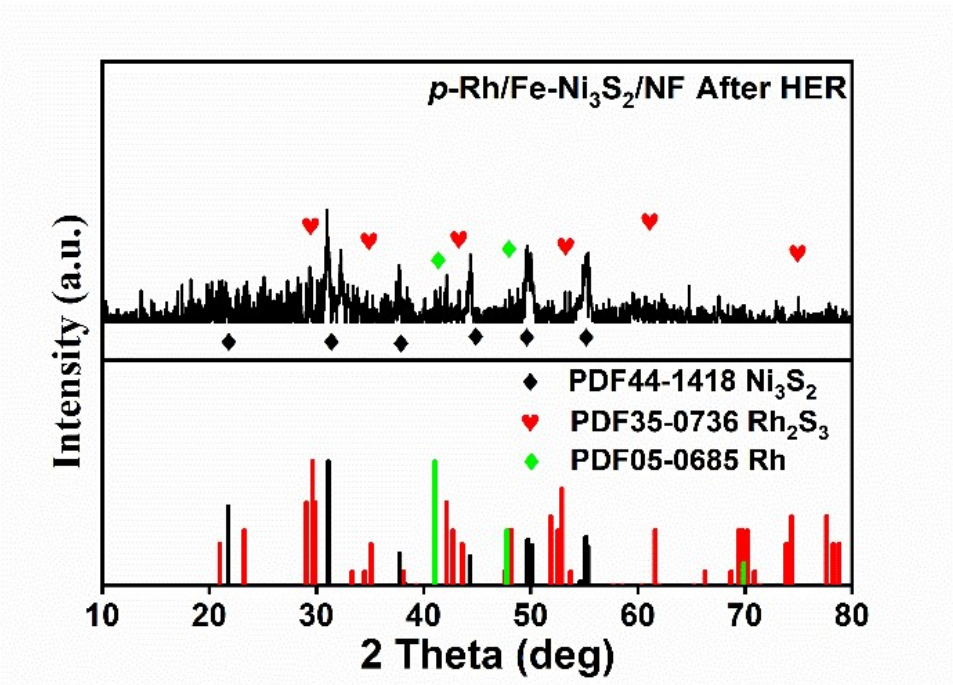

Fig. S14. XRD pattern of *p*-Rh/Fe-Ni_3S_2/NF after 50 h HER at 100 mA cm^{-2}.

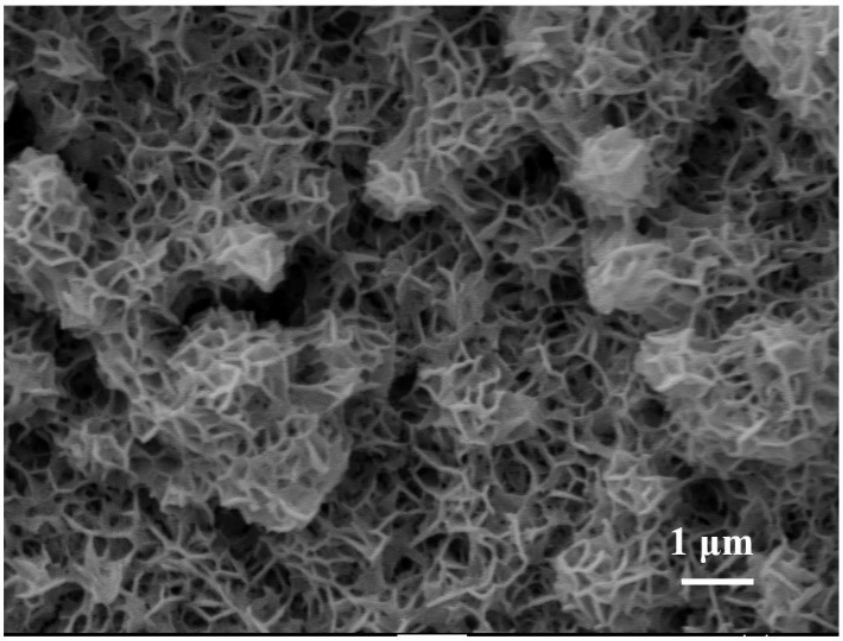

Fig. S15. SEM image of *p*-Rh/Fe-Ni_3S_2/NF after 50 h HER at 100 mA cm^{-2}.

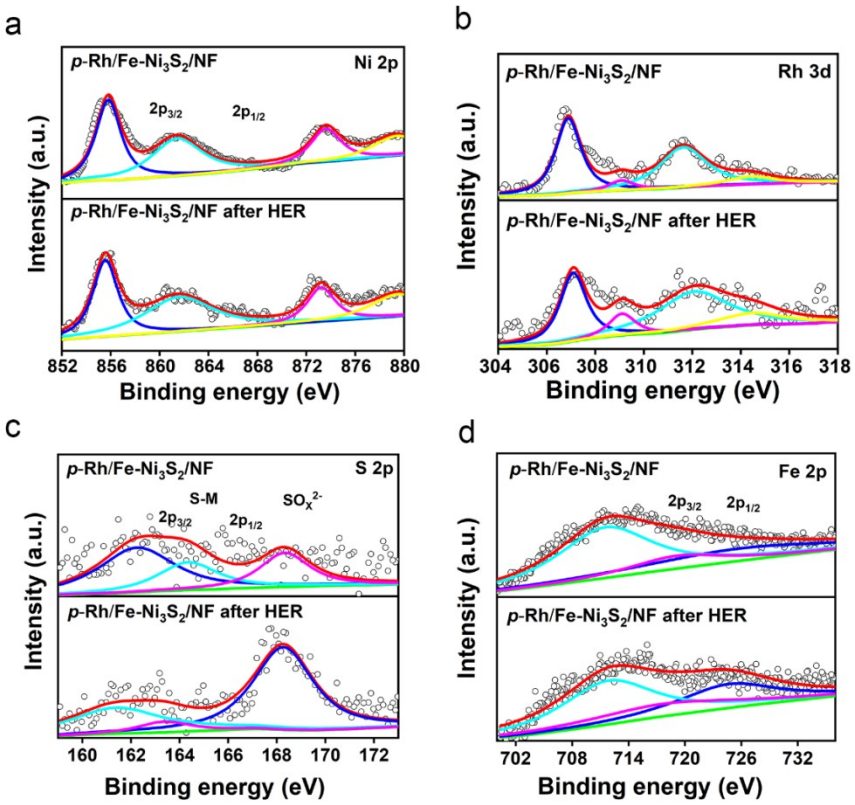

Fig. S16. XPS survey spectra and (a) Ni 2p spectra (b) Rh 3d spectra (c) S 2p spectra and (d) Fe 2p spectra of *p*-Rh/Fe-Ni_3S_2/NF after 50 h HER at 100 mA cm^{-2}.

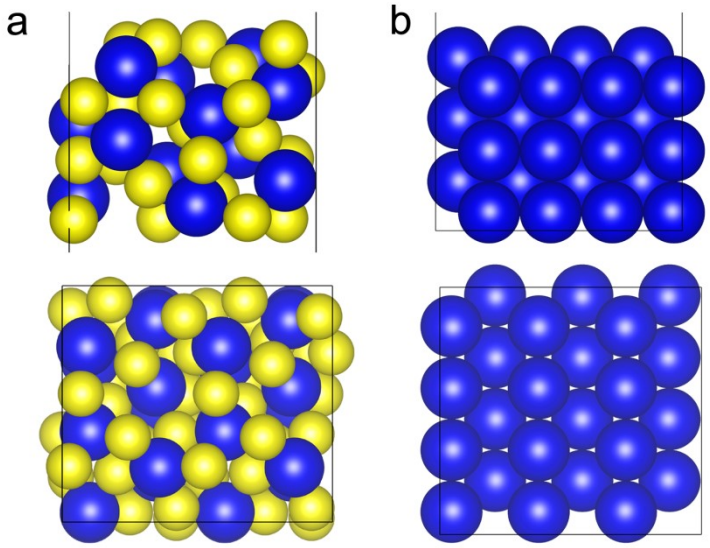

Fig. S17. (a) Side (upper) and top view (bottom) of the model surface of pure Rh (a) and pure Rh_2S_3. Bule and yellow balls represent Rh and S atoms, respectively.

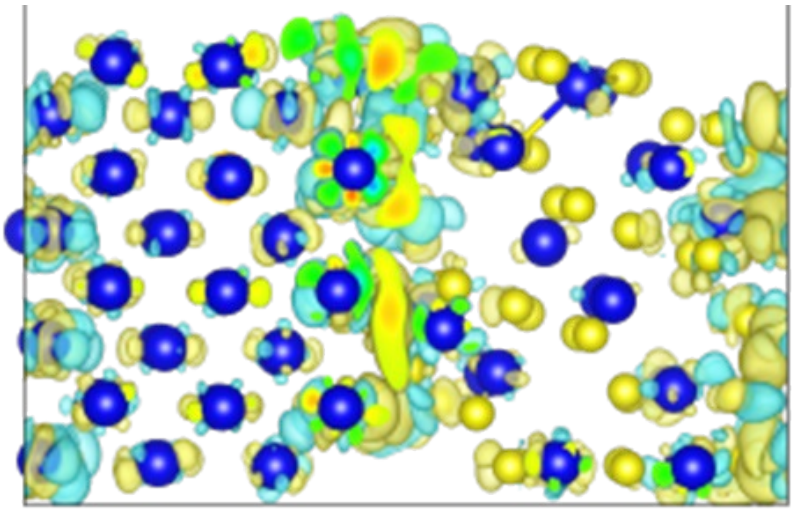

Fig. S18. The charge density difference of Rh_2S_3/Rh interface. Bule and yellow balls represent Rh and S atoms, respectively.

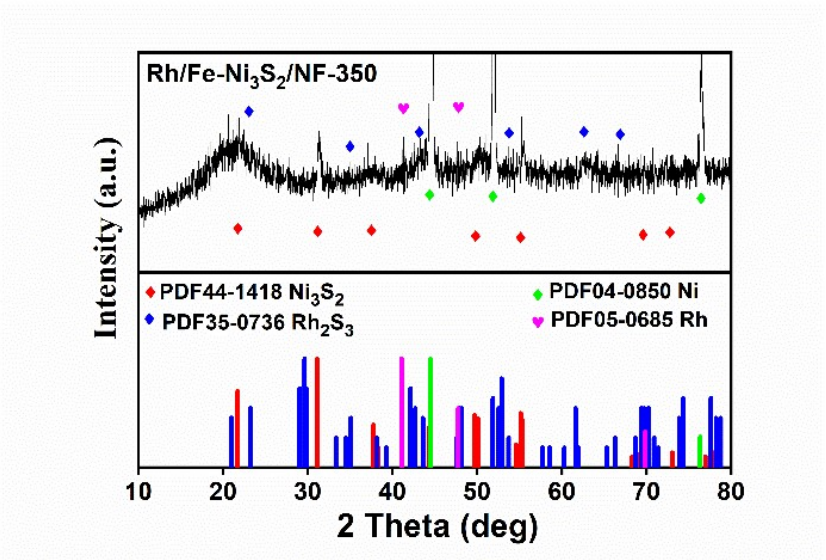

Fig. S19. XRD pattern of Rh/Fe-Ni_3S_2/NF-350 synthesized with thermal reduction of Rh/Fe-Ni_3S_2/NF precursor in H_2/Ar at 350 ℃.

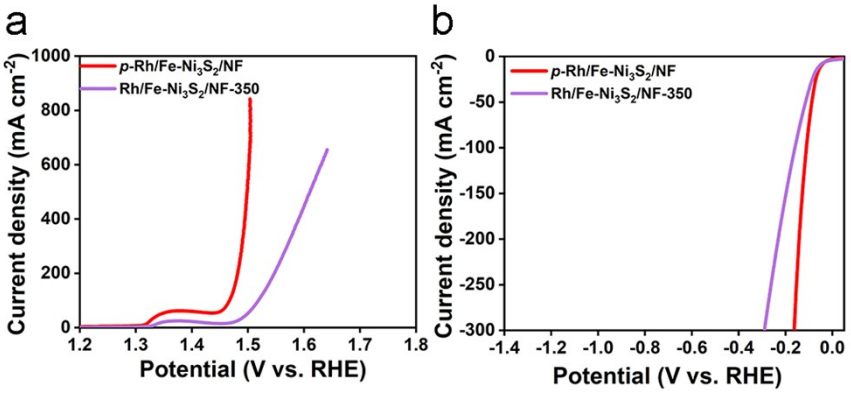

Fig. S20. OER performance (a) and HER performance (b) of *p*-Rh/Fe-Ni_3S_2/NF and Rh/Fe-Ni_3S_2/NF-350 in 1 M KOH.

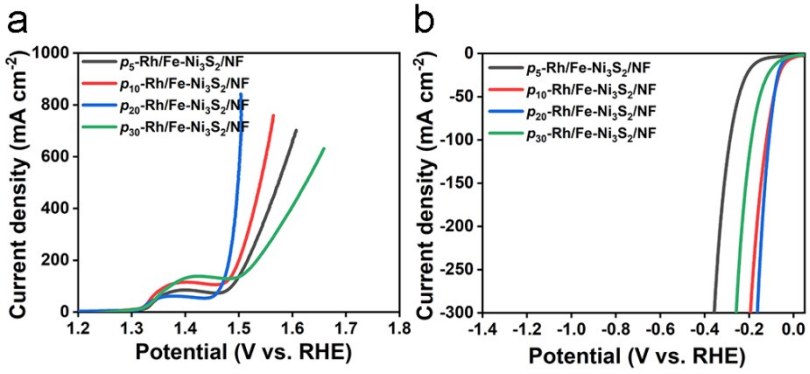

Fig. S21. OER (a) and HER performance (b) of *p*-Rh/Fe-Ni_3S_2/NF synthesized with H_2 plasma treatment of different durations in 1 M KOH. The duration is 5, 10, 20, and 30 min for p5-Rh/Fe-Ni_3S_2/NF, p10-Rh/Fe-Ni_3S_2/NF, p20-Rh/Fe-Ni_3S_2/NF and p30-Rh/Fe-Ni_3S_2/NF.

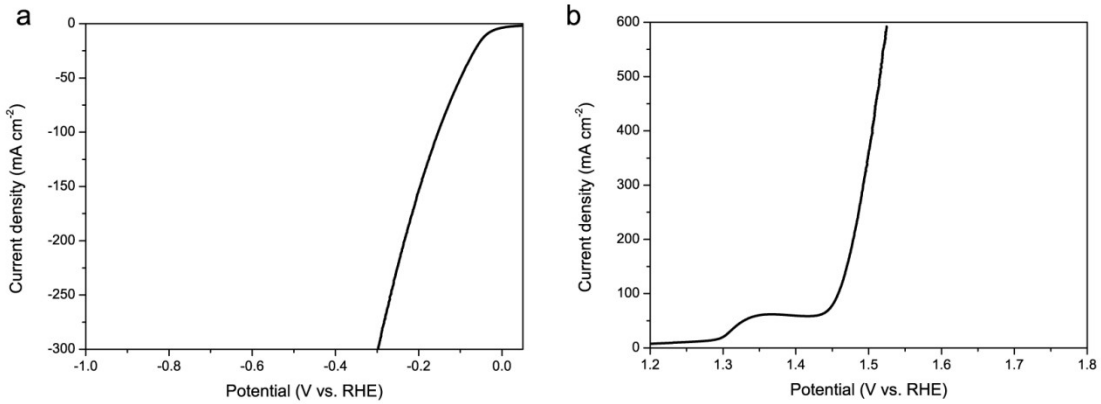

Fig. S22. HER (a) and OER performance (b) of Rh/Fe-Ni_3S_2/NF after 30 min Ar plasma treatment in 1 M KOH. Both HER and OER activity were slightly enhanced compared to Rh/Fe-Ni_3S_2/NF but are inferior to *p*-Rh/Fe-Ni_3S_2/NF, indicating the important role of hydrogen plasma.

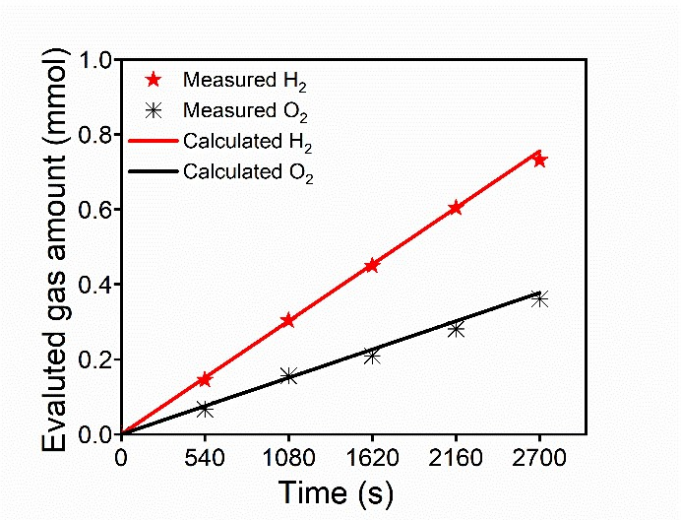

Fig. S23. Volume of gas theoretically calculated and experimentally measured versus time on *p*-Rh/Fe-Ni_3S_2/NF.

Reference

1. Wang L, Wu H, Xi S, et al. Nitrogen-doped cobalt phosphide for enhanced hydrogen evolution activity. ACS Appl. Mater. Interfaces. 2019, 11, 17359-17367.

2. Cao E, Chen Z, Wu H, et al. Boron-induced electronic-structure reformation of cop nanoparticles drives enhanced ph-universal hydrogen evolution. Angew. Chem. Int. Ed. 2020, 59, 4154-4160.

3. Luo M, Wang Z, Li YC, et al. Hydroxide promotes carbon dioxide electroreduction to ethanol on copper via tuning of adsorbed hydrogen. Nat. Commun. 2019, 10, 5814.

4. Isabela C. Man, Hai-Yan Su, Federico Calle-Vallejo, et al. Universality in Oxygen Evolution Electrocatalysis on Oxide Surfaces. 2011, 3, 1159-1165.